CrystEngComm

PAPER

View Article Online
View Journal | View Issue

Cite this: *CrystEngComm*, 2015, **17**, 2389

Polymorphism and solid-to-solid phase transitions of a simple organic molecule, 3-chloroisonicotinic acid†

Sihui Long,‡[a] Panpan Zhou,‡[b] Sean Parkin[c] and Tonglei Li*[d]

Received 30th December 2014,
Accepted 5th February 2015

DOI: 10.1039/c4ce02563f

www.rsc.org/crystengcomm

Three polymorphs (I, II, and III) have been discovered for 3-chloroisonicotinic acid. The torsion angle between the aromatic ring and the carboxylic acid in form I differs from that of forms II and III, which are similar. All three polymorphs form hydrogen-bonded chains based on the acid–pyridine heterosynthon. Despite the conformational similarity between forms II and III, the hydrogen-bonded chains in form II alternate in direction while those in form III all point in the same direction. Study of the phase behaviors of the three forms by differential scanning calorimetry, hot-stage microscopy, and thermogravimetric analysis revealed two solid-to-solid phase transitions from the metastable forms II and III to the most stable form I. Sublimation of 3-chloroisonicotinic acid also led to form I. A higher-temperature polymorph seemed to be possible but remained elusive. Lattice energy and hydrogen bonding strength calculations provided further insight into the stability of the polymorphs. A search of conformational space for the molecule suggested possibly additional polymorphs of this simple compound. The system may be valuable for further solid-state structure–property relationship studies.

1. Introduction

Polymorphism, the phenomenon in which a compound exists in multiple crystal structures, has been routinely observed in the studies of organic materials.[1–6] Despite numerous cases of polymorphism, the underlying mechanism of the phenomenon is not fully understood; the practical task of polymorph control is still daunting, and accurate routine crystal structure prediction remains elusive. Nevertheless, the challenges propel advances in the field as we gain insight into the nucleation mechanism[7–11] and witness new polymorph control methods,[12] such as application of additives,[13] use of polymers to induce heteronucleation,[14] use of self-assembled monolayers,[15,16] and practice of non-photochemical laser-induced nucleation,[17] emerging in the past decade. An increasing number of successful cases of crystal structure prediction, exemplified by the blind tests of organic crystal structure prediction organized by the Cambridge Crystallographic Data Centre (CCDC) as well as individual efforts,[18–24] exemplify successes and pitfalls in understanding crystallogenesis. Clearly, the polymorphism of an organic system yields a fundamental glimpse into the structure–property relationships involved in molecular packing. Studies of polymorphs can thus lead to the buildup and generalization of crystallization principles, deepening our knowledge in understanding molecular interactions. As a special class of polymorphism, the difference in molecular conformation among polymorphs of a compound offers an excellent platform for comprehending the complexity imposed by the intra- and intermolecular interactions on the self-assembling process of crystallization.[25–27]

To systematically study crystal packing of organic molecules, we have resorted to diarylamines derived from nicotinic acid as a platform to understand intermolecular interactions and roles played by solvents and additives in manipulating the formation of crystal structures. These compounds have both carboxyl and pyridinyl functional groups and are structurally flexible, and therefore amendable to polymorphism. A series of compounds have been studied, and these include 2-(phenylamino)nicotinic acid (2-PNA) and 2-[methyl(phenyl)amino]nicotinic acid (2-MPNA) as well as other structurally similar compounds.[28–30] The majority of

[a] *School of Chemical Engineering and Pharmacy, Wuhan Institute of Technology, Wuhan, Hubei, China*
[b] *Department of Chemistry, Lanzhou University, Lanzhou, Gansu, China*
[c] *Department of Chemistry, University of Kentucky, Lexington, Kentucky 40506, USA*
[d] *Department of Industrial and Physical Pharmacy, Purdue University, 575 Stadium Mall Drive, West Lafayette, Indiana 47907, USA. E-mail: tonglei@purdue.edu; Tel: +1 765 494 1451*

† Electronic supplementary information (ESI) available: Crystal structures of the three polymorphs in the form of the crystallographic information file (CIF). Additional PXRD and DSC data. CCDC 1041847, 1041848 and 1041849. For ESI and crystallographic data in CIF or other electronic format see DOI: 10.1039/c4ce02563f

‡ S. L. and P. Z. contributed equally.

the compounds were found to be polymorphic likely due to both the molecular flexibility and the competition between the acid–pyridine heterosynthon and the acid–acid homosynthon. For example, 2-PNA and 2-MPNA were found to be highly polymorphic with each forming at least four crystal structures, and interesting phase behaviors such as solid-to-solid phase transitions were also observed.[28,29] By introducing electron withdrawing groups or bulky substituent groups onto the benzene ring, a planar conformation favoring the acid–acid dimer by excluding the acid–pyridine interaction or a twisted conformation preferring the acid–pyridine hydrogen bonding could be realized for these diarylamines.[31,32] Recently, a molecule in which both acid–pyridine and acid–acid hydrogen bonding motifs coexisted was designed.[33] The acid–pyridine hydrogen bond was found to be stronger than the acid–acid interaction and thus should be predominant in simple molecules such as nicotinic acid and its isomers as well as halogenated nicotinic acids and isonicotinic acids. Herein, we report a study of the solid forms of 3-chloroisonicotinic acid (3-CINA) (Fig. 1), an important building block of organic synthesis and pharmaceuticals,[34] and a simple compound with both carboxylic acid and pyridine functionality. The crystal structure of 3-CINA is expected to include acid–pyridine hydrogen bonding due to the aforementioned reason. Nonetheless, three polymorphs (I, II, and III) were discovered at room temperature from crystal growth in different solvents. The torsion angles between the aromatic ring and the carboxylic acid group in forms II and III are similar but quite different from that of form I. The hydrogen bonding patterns of all three forms are different although they are based on the same acid–pyridine heterosynthon. Interesting solid-state phase behaviors were discovered. Lattice energy and hydrogen-bond strength calculations provided insight into the relative stability of the three forms, and a conformation search suggested possible new modifications.

2. Experimental and computational procedures

2.1. General

3-CINA (97% purity) was purchased from Aldrich. All solvents were obtained from commercial sources and used as received. Thermal analyses were performed by differential scanning calorimetry (DSC, TA Instruments Q20), thermogravimetric analyses (TGA, TA Instruments Q50), and hot-stage microscopy (HSM, INSTEC STC200). For the DSC and TGA experiments, Tzero® pans and aluminum hermetic lids were used for measuring, generally, a few milligrams of samples at a heating rate of 10 °C min^{-1}.

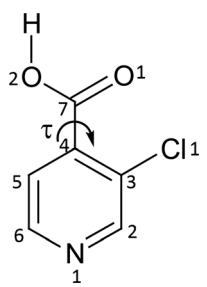

Fig. 1 3-Chloroisonicotinic acid. The torsion angle used in the conformation search is marked by τ (defined by O1C7C4C5).

2.2. Crystal growth

3-CINA was dissolved in different solvents (water, methanol, ethanol, acetone, acetonitrile, dimethylsulfoxide, and dimethylformamide) forming clear solutions at room temperature. The solutions were set for slow evaporation until single crystals formed. They were harvested either with residual solvent or after complete solvent evaporation. All crystallization experiments were conducted in an unmodified atmosphere. A typical protocol was performed in which 50 mg of 3-CINA was dissolved in 10 mL of high-performance liquid chromatography (HPLC) grade methanol in a glass vial at room temperature. Vials were covered with a perforated parafilm.

2.3. Crystal structure determination

Crystal structures of 3-CINA were determined by single-crystal X-ray diffraction (SXRD). For the crystals measured, data collection was carried out at 90 K using a Nonius kappa CCD diffractometer with Mo Kα radiation (λ = 0.71073 Å).[35] Cell dimensions and data reduction were conducted with SCALEPACK in DENZO-SMN.[36] Structure solution and refinement were completed with SHELXS97 and SHELXL97, respectively.[37]

Powder X-ray diffraction (PXRD) for each sample was performed with a Rigaku X-ray diffractometer with Cu Kα radiation (40 kV, 44 mA, and λ = 1.5406 Å) from 5.0 to 50.0° (2θ) at room temperature. Each sample was ground and then placed on a quartz plate in an aluminum sample holder.

2.4. Conformational search and hydrogen bonding energy

To investigate the conformation in the crystal structures, the energy of a single 3-CINA molecule as a function of the torsion angle τ (Fig. 1) was evaluated using the Gaussian 09 programs.[38] The most stable conformer was identified first by comparing optimized structures from various initial structures with subsequent variation of the torsion angle with all bond lengths and bond angles fixed. Basis sets at the B3LYP/6-311G(d,p) and B3LYP/6-311++G(d,p) levels of theory were used for the structural optimization and conformational search, respectively. To estimate binding strengths between molecules in the crystal, the hydrogen-bonded dimers in the three forms were evaluated. The dimers were taken from the three crystal structures, and then the coordinates of the atoms except for H atoms were kept frozen for structural optimization at the M062X/6-31+g(d,p) level of theory. The M062X method was chosen because of its accuracy in treating non-covalent interactions and computational efficiency.[39–41] The interaction energies (ΔE) of the dimers were calculated

as the energy difference between the total energy of the dimer and the sum of total energies of its constituent molecules.

2.5 Lattice energy calculation

Lattice energy defines the stability of an organic crystal. To investigate the relative stability of crystal structures obtained, lattice energies were evaluated by periodic DFT (density functional theory) methods augmented by long-range van der Waals energies and analytical energy models based on interatomic distances and pre-defined parameters.[42,43] Previous results of dozens of organic crystals calculated by this method were in good agreement with experimental values.[42,43]

A periodic quantum mechanics program, Crystal 06,[44] was used for optimization and energy calculation of crystals and single molecules. The unit cell parameters were kept constant during the optimization of the crystal structures. The basis set superposition error (BSSE) was corrected by using the counterpoise method.[45] The basis set used was B3LYP/6-21G-(d,p) for optimization and B3LYP/6-31G(d,p) for single point energy calculation and BSSE. No diffusion function was included due to the periodicity of Bloch functions for constructing the local functions of the DFT calculations. The energy convergence of the optimizations and energy calculations was set to 10^{-7} Hartree. Root-mean-squares (RMS) were set to 0.0003 and 0.0012 atomic units for energy gradient and atomic displacement, respectively.

3. Results and discussion

Three polymorphs (I, II, and III) were produced from the seven solvents used. The polymorphs showed poor solvent selectivity in acetone, methanol and water as all three forms were accessible from acetone individually and sometimes concomitantly, forms I and II could be obtained from methanol, and forms II and III were harvested from water. Form I was also prepared from acetonitrile and dimethylsulfoxide, form II from ethanol, and form III from dimethylformamide (Table 1). Single crystals of forms I, II, and III for structure determination were grown in acetone, methanol, and water, respectively. Some representative crystals of the three forms are illustrated in Fig. 2.

Table 1 Crystal growth of 3-CINA in different solvents and under different conditions

Solvent	Growth condition	Polymorph
Methanol	Slow evaporation	I, II
Methanol	Slow cooling	I
Ethanol	Slow evaporation	II
Water	Slow evaporation	II
Water	Slow cooling	III
Acetone	Slow evaporation	I, II, III
Acetone	Slow cooling	I
Acetonitrile	Slow evaporation	I
Dimethyl sulfoxide	Slow evaporation	I
N,*N*-Dimethylformamide	Slow evaporation	III

3.1. Crystal structures

Structure determination by SXRD shows that form I is triclinic with space group $P\bar{1}$ ($Z = 2$), form II is monoclinic with $P2_1/n$ ($Z = 4$), and form III is triclinic with $P1$ ($Z = 1$). Details of the lattice parameters and measurement conditions are summarized in Table 2. CIF files can be found in the ESI.† Careful examination of the crystallographically independent molecules in the asymmetric units ($Z' = 1$ in each polymorph) shows conformational differences. The difference between the three conformations lies in the torsion angle τ between the carboxylic acid and the aromatic ring (*ca.* 163.9° in form I, −144.9° in form II, and −142.5° in form III). Superposition of the conformations indicates the conformational difference, as shown in Fig. 3. Thus, at first sight, this system seems to be of pure conformational polymorphism albeit the small conformational difference between forms II and III. Yet, analysis of the packing patterns of all three forms revealed a major difference between form III and forms I and II. In all three forms the carboxylic acid has the *syn* conformation,[46–48] and all three polymorphs form one-dimensional hydrogen-bonded chains (these hydrogen bonding chains are along the *c* axis in form I, parallel to the (010) plane in form II, and parallel to the (110) plane in form III) incorporating the acid–pyridine heterosynthon (C(7) by the graph set designation).[49] The acid–acid homosynthon is not observed, which is in agreement with the fact that the acid–pyridine heterosynthon is energetically favored over the acid–acid homosynthon. The direction of hydrogen-bonded chain propagation alternates in forms I and II, while in form III, all the hydrogen bonding chains point to the same direction, resulting in a non-centrosymmetric crystal (Fig. 4). This is similar to the polymorphic system of 2-MPNA whose four forms stem from the directionality of hydrogen-bonded chains in the crystals.[28] In addition, because of the conformational difference, the length and angle of the hydrogen bond in the three polymorphs vary. The OH···N hydrogen bond distance and angle are 2.6264(15) Å and 174.1(1)° in form I, 2.6390(14) Å and 172.9(4)° in form II, and 2.613(2) Å and 171.9(1)° in form III, respectively. Nonetheless, the differences in the hydrogen bonds seem to be insignificant.

The conformational difference is manifest as a rotation around the C–C bond between the aromatic ring and the carboxylic acid. The C–C bond between the –COOH and the pyridine ring of the conformations is essentially single, as indicated by the bond length (*ca.* 1.51 Å). This suggests that the –COOH is no longer in tight conjugation with the aromatic ring as indicated by τ and the rotation about the C–C bond is permitted to some extent. Fig. 5 shows the energy scan of various conformations of τ, indicating that the global minimum resides at ±180° and the local minimum at ±47.5°. The energy difference between the two minima is about 4.4 kJ mol^{-1}, while the maximum at 0° is due to repulsion between Cl and

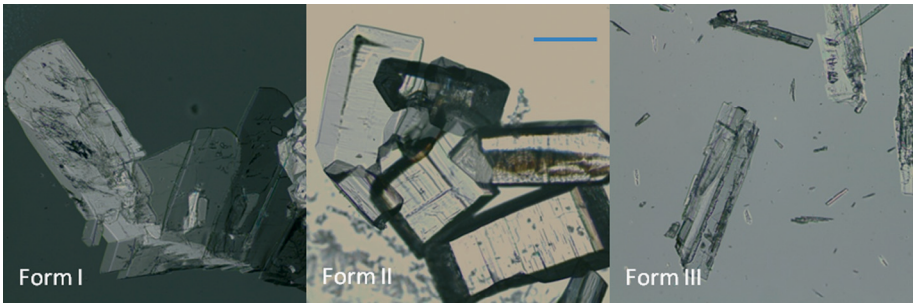

Fig. 2 Crystals of the three polymorphs (I, II and III) of 3-CINA. Scale bar: 0.3 mm.

C═O. The energy curve suggests no significantly large energy barrier exists, so it is expected that the 3-CINA molecule could traverse a large range of energy space defined by τ. The energy difference among the three conformations in the polymorphic structures is smaller than 2 kJ mol^{-1}. Despite the conformational difference, the crystal structures of 3-CINA are likely determined by intermolecular interactions and hydrogen-bonding patterns, facilitated by kinetic factors including use of different solvents. The difference in the torsion angle is undoubtedly a result of the crystal packing. Because there are no high energy barriers on the energy curve, it is possible that more polymorphic structures of 3-CINA exist (as suggested later, a high-temperature polymorph may exist).

In contrast, isonicotinic acid has only one known crystal structure,[50] in which the molecule takes a planar conformation and forms the same hydrogen-bonding chain as 3-CINA (Fig. 4). The absence of a substituent at the *ortho* position to the carboxylic acid renders the planar conformation the most stable and the only viable choice for the intermolecular packing. Conversely, the presence of chlorine forces the 3-CINA molecule to twist weakening the conjugation between the carboxyl and pyridinyl groups. This, shown in Fig. 4, introduces the packing diversity simply because the symmetry inherent to isonicotinic acid no longer exists. For the same conformational energy, the molecule can take the same torsion angle (τ, Fig. 1) but of the opposite sign, thereby leading to polymorphism. Along the hydrogen-bonded chain, the torsion angle is positive in form I, and both positive and negative in form II, and negative in form III. It may thus be concluded that the polymorphism of 3-CINA is a result of disruption of the molecular symmetry by chlorine substitution. Interestingly, an isonicotinic acid derivative with two chlorine substituents at the symmetric 2 and 6 positions has just one crystal structure reported (CSD refcode: XEPRIU), seemingly supporting the formation of multiple crystal forms of 3-CINA.

Table 2 Crystallographic data of three polymorphs of 3-CINA

Form	I	II	III
Formula	$C_6H_4ClNO_2$	$C_6H_4ClNO_2$	$C_6H_4ClNO_2$
Formula weight	157.55	157.55	157.55
Crystal size (mm)	0.60 × 0.15 × 0.08	0.50 × 0.20 × 0.15	0.40 × 0.20 × 0.10
Crystal system	Triclinic	Monoclinic	Triclinic
Space group	$P\bar{1}$	$P2_1/n$	$P1$
a/Å	7.1603(2)	7.3267(2)	3.67790(10)
b/Å	7.2376(2)	6.6413(2)	6.93710(10)
c/Å	7.4950(3)	12.6512(4)	7.0372(2)
α/°	63.2313(14)	90	61.6975(14)
β/°	69.7053(14)	92.2254(15)	80.0002(12)
γ/°	64.9840(15)	90	89.5122(12)
Z, Z'	2, 1	4, 1	1, 1
V/Å^3	308.331(17)	615.13(3)	155.117(6)
D_{cal}/g cm^{-3}	1.697	1.701	1.687
T/K	90.0(2)	90.0(2)	90.0(2)
Abs coeff (mm^{-1})	0.541	0.542	0.538
F(000)	160.0	320.0	80.0
θ range (deg)	3.10–27.43	3.16–27.48	5.88–27.49
Limiting indices	$-9 \le h \le 9$ $-9 \le k \le 9$ $-9 \le l \le 9$	$-9 \le h \le 9$ $-8 \le k \le 8$ $-16 \le l \le 16$	$-4 \le h \le 4$ $-8 \le k \le 8$ $-9 \le l \le 9$
Completeness to 2θ	99.9%	99.5%	100.0%
Unique reflections	1263	1284	1332
$R_1[I > 2\sigma(I)]$	0.0313	0.0254	0.0164
wR_2 (all data)	0.0848	0.0764	0.0461

3.2. Thermal analyses

DSC and TGA results of the three polymorphs of 3-CINA are illustrated in Fig. 6. The measurements were conducted in hermetically sealed aluminum pans. Form I shows two endothermic DSC phenomena with onset temperatures at 220.5 and 230.4 °C (see the ESI† for additional DSC results including at variable scanning rates, 1 and 30 °C min^{-1}, and by modulated temperature DSC). Form II shows three endothermic DSC events with the onset temperature of the first one at

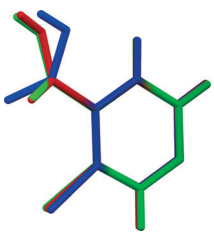

Fig. 3 Superposition of three conformations in forms I–III (I, blue; II, red; and III, green).

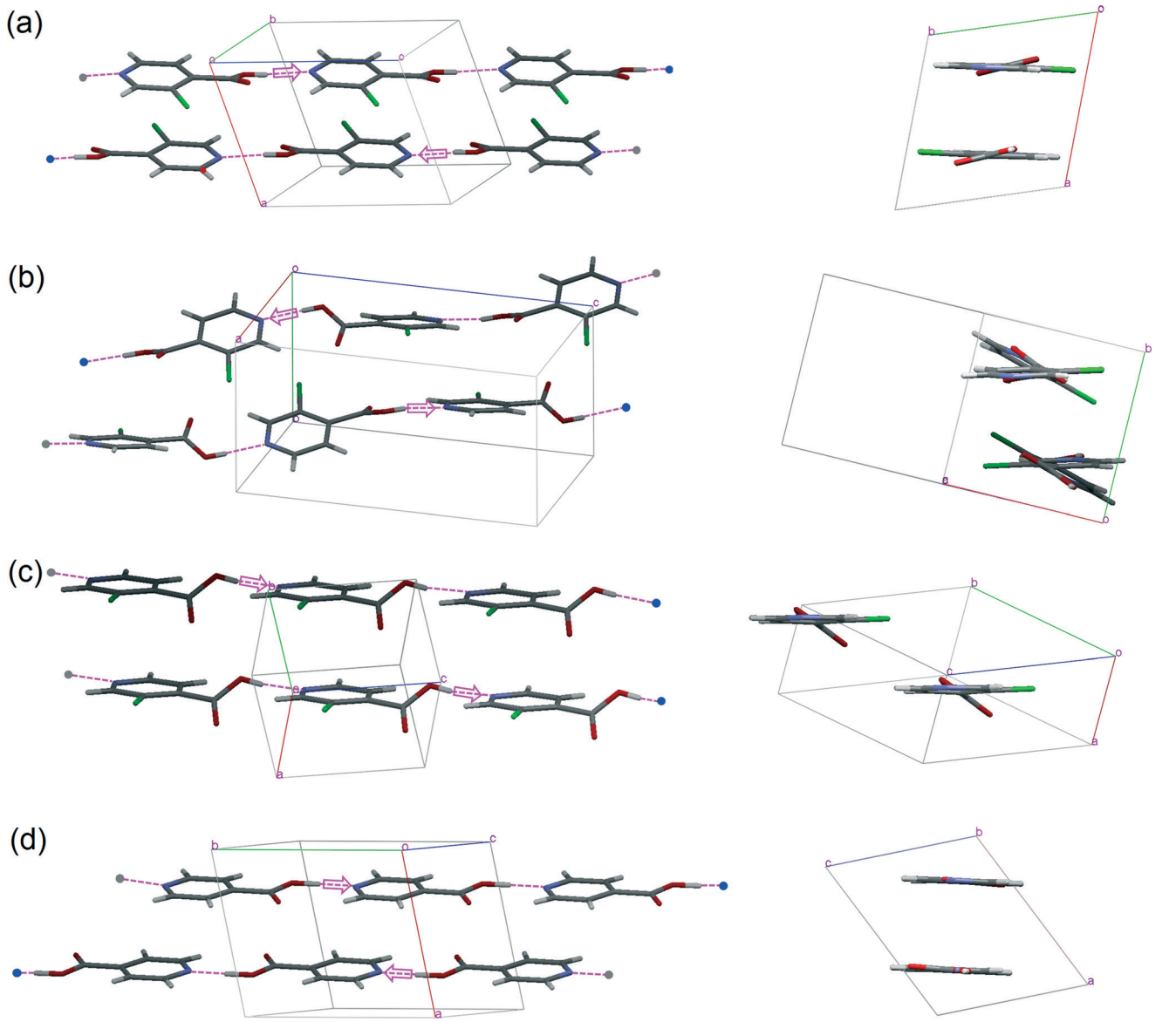

Fig. 4 Different views for crystal packing of forms I (a), II (b), and III (c) of 3-CINA, and isonicotinic acid (d). Hydrogen bonds are highlighted with dashed lines, and the arrows indicate the hydrogen-bonding directions (from donor to acceptor).

138.3 °C; the other two are 221.7 and 229.8 °C, respectively. The thermal behaviors of form III resemble those of form I with two endothermic DSC events, with onset temperatures at 222.3 and 230.0 °C, respectively.

To understand the nature of the first endothermic event of form II, hot-stage microscopy was employed. Samples of form II crystals were placed on the hot stage and heated up to 140 °C, and a solid-to-solid phase transition was observed, as illustrated in Fig. 7. It should be noted that the heating rate of HSM was 1 °C min^{-1} while that of DSC in Fig. 6 was 10 °C min^{-1}; the difference may explain why the phase transition was complete before 140 °C in Fig. 7 but not until 160 °C in Fig. 6. The resultant crystals were polycrystalline and were verified by PXRD as form I (Fig. 8). The quality of crystals and preferred orientation may account for the missing peaks in the experimental PXRD patterns. Peak shifting between the simulated and experimental patterns of form II is likely due to the temperature difference since the structure was solved at 90 K. And the discrepancy of form I could be due to the same reasons, as well as possible presence of residual form II. Thus, form II of 3-CINA can initiate solid-to-solid phase transition to form I below 140 °C. Clues to the solid-to-solid phase transition may be found in the similar packing features of these two polymorphic structures. Despite their different conformations, the molecules in the two forms interact in a similar fashion, based on the acid–pyridine heterosynthon. When energy is provided by heating, the rotation of the single bond between the aromatic ring and the carboxyl may facilitate the phase transition *via* a nucleation-and-growth mechanism as observed in Fig. 7b–d.

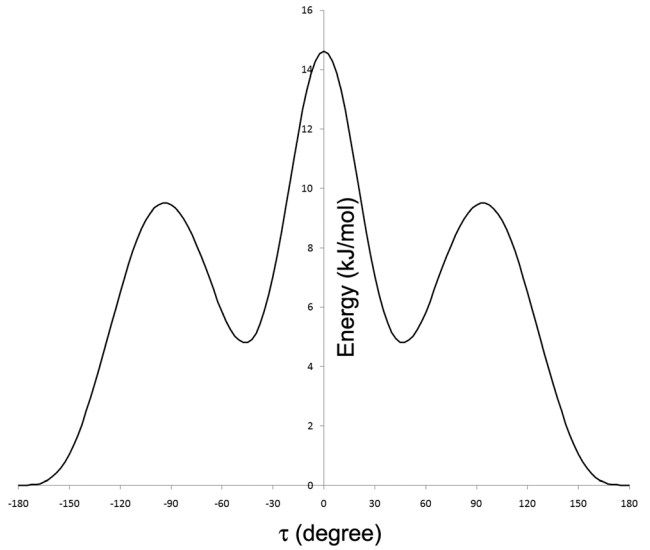

Fig. 5 Energy of a 3-CINA single molecule as a function of torsion angle τ relative to the lowest-energy conformer.

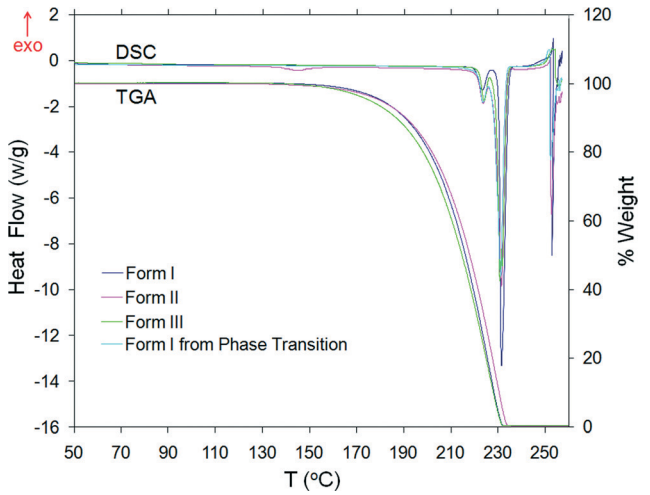

Fig. 6 DSC and TGA thermograms of the three polymorphs. TGA were run in open DSC pans. Form I converted from form II is also shown in DSC.

Examination of the DSC traces of forms III and I seems to indicate that they were identical. This lack of phase transition was initially thought to be a case of iso-energetic polymorphism. Yet, HSM study with single crystals of form III revealed a solid-to-solid phase transition, similar to that of form II. The resulting polycrystalline product was again confirmed by PXRD to be form I (Fig. 9). The absence of an observable phase transition peak by DSC could be due to the minute energy involved. This was later proven by another set of DSC runs for form III samples (5 repeats) (Fig. 10). The onset temperature of the phase transition was found to be ~160 °C, with an enthalpy of only 0.454 (0.112) J g^{-1}.

The DSC peak at around 220 °C could be from another phase transition from form I to a high temperature form. This unknown form then melts and partially decomposes at

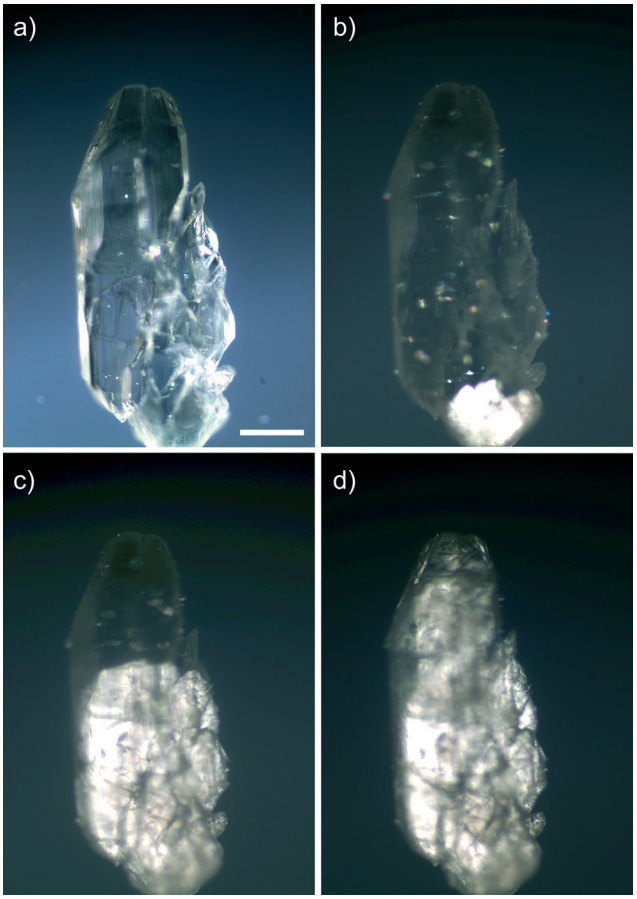

Fig. 7 Solid-to-solid phase transition of form II to form I observed by hot-stage microscopy during heating: 91.2 (a), 133.0 (b), 134.4 (c), and 135.7 °C (d). Scale bar: 0.2 mm.

230 °C. Efforts to preserve the possible new form for structure determination were unsuccessful.

Sublimation of each polymorph was detected above 120 °C when a crystal was put on the hot stage. New crystals were readily formed at the cover glass of the hot stage due to cooling of the gaseous molecules. Interestingly, form I crystals were always collected at the cover glass no matter which polymorph was heated. The sublimation was confirmed by TGA with the sample pans uncovered (Fig. 6). At about 230 °C, the samples were completely vaporized.

3.3. Lattice energy and hydrogen-bonding strength

The calculated lattice energies based on the empirically augmented DFT method were −109.321, −108.852 and −106.071 kJ mol^{-1} for forms I, II and III, respectively. The results suggest the stability order to be I > II > III with form I being the most stable, as supported by the experimental data. Energy values of forms I and II are extremely close (within 1 kJ mol^{-1}), further suggesting that solid-to-solid phase transition from form II to form I is likely. Nonetheless, the small energy difference between forms I and II should not be regarded as evidence of which one is more stable, especially given the

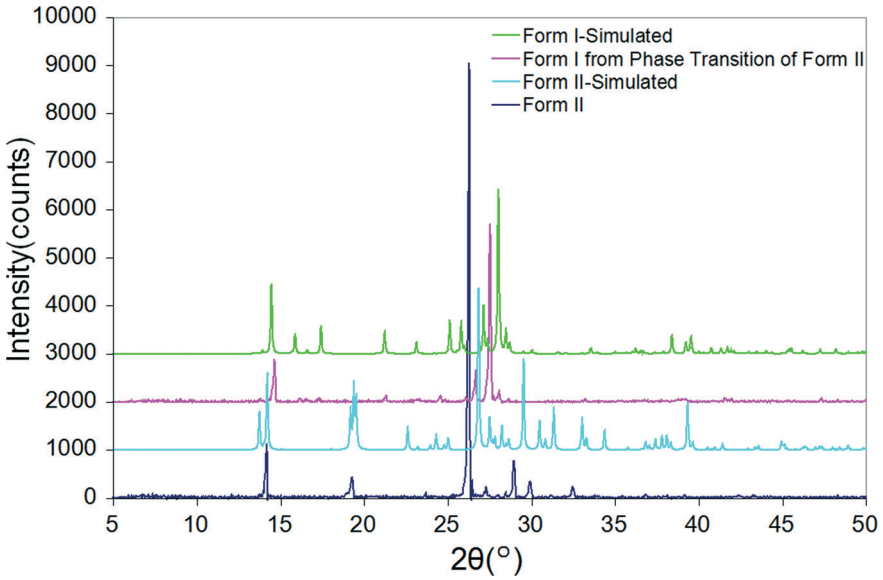

Fig. 8 PXRD of form II before and after the solid-to-solid phase transition.

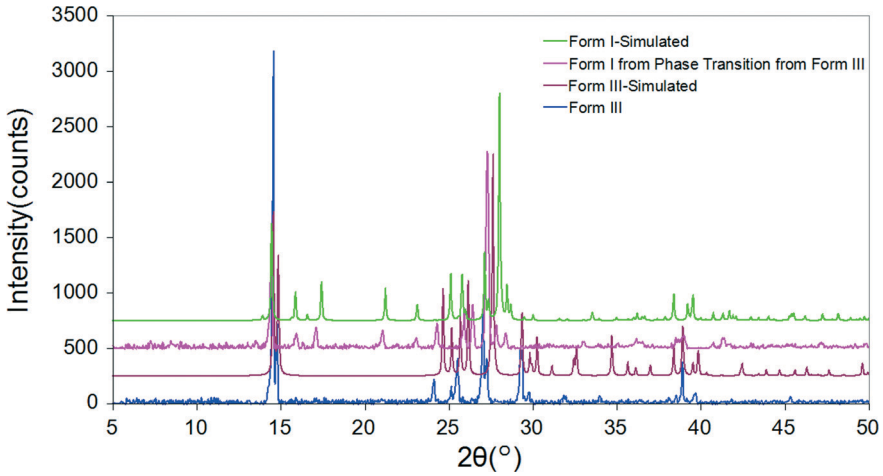

Fig. 9 PXRD of form III before and after the solid-to-solid phase transition.

uncertainty limit inherent to the computation methods employed (which may range from a few kilojoules per mole to a few kilocalories per mole or even higher). The density values do suggest a ranking order of forms II > I > III with form II being the densest (Table 2). It should be pointed out that the computation was implicitly conducted at zero Kelvin and the density values are based on the structures measured at 90 K. As such, whether the system is enantiotropic deserves further investigation.

In addition, the hydrogen-bonding strengths for the dimers in forms I, II and III were evaluated. The results show that the acid–pyridine hydrogen-bonding (N···H–O) dimer in form II is the strongest (−43.72 kJ mol^{-1}), followed by that in forms I (−40.80 kJ mol^{-1}) and III (−36.24 kJ mol^{-1}). It is different from the stability order of the lattice energies as well as the experimental data, indicating that the crystal is stabilized not only by the hydrogen-bonding interactions, but also obviously by other interactions including van der Waals interactions and close contacts as well.

4. Conclusions

Three polymorphs of 3-CINA, a simple organic molecule, were identified by crystallization from different solvents. Solid-to-solid phase transitions from forms II and III to form I and sublimation of all three forms were observed, and form I appeared to be the more stable form at temperatures higher than the transition temperatures. An additional high-temperature form was also inferred. Information regarding the relative stability of the three forms and the underlying mechanism was gained through theoretical calculations including lattice energy evaluation and hydrogen bonding strength comparison. Given the conformational flexibility of the molecule, a relatively low energy barrier on the

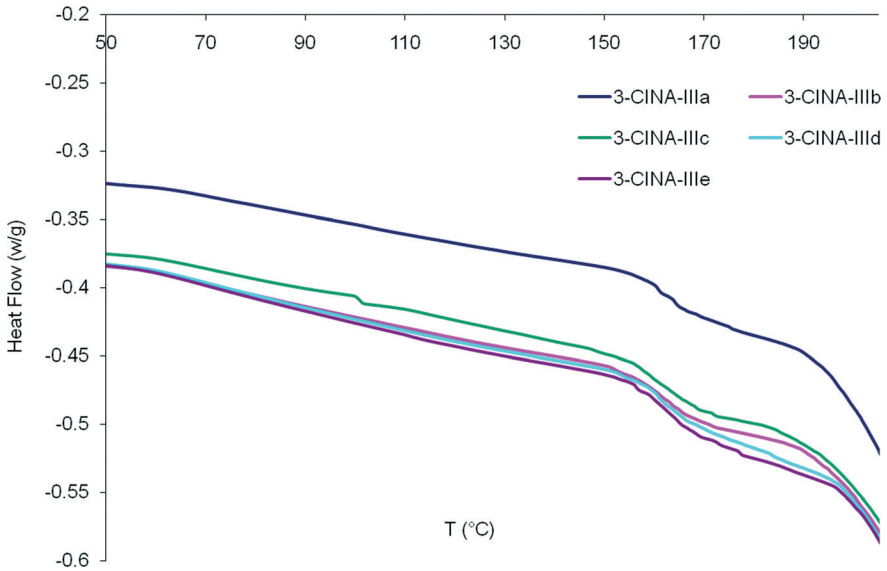

Fig. 10 DSC thermograms of form III (five repeats).

conformational energy curve (Fig. 3), and disrupted molecular symmetry by the chlorine substituent, more polymorphs are expected.

Acknowledgements

SL thanks the Natural Science Foundation of Hubei Province for financial support (2014CFB787). PPZ thanks the financial support by the National Natural Science Foundation of China (grant no. 21403097) and the Fundamental Research Funds for the Central Universities (lzujbky-2014-182). TL is grateful to NSF for supporting the work (DMR1006364).

References

1 J. Bernstein, *Polymorphism in Molecular Crystals*, Oxford University Press, New York, 2002.
2 H. G. Brittain, *Polymorphism in Pharmaceutical Solids*, Marcel Dekker, New York, 1999.
3 H. G. Brittain, *J. Pharm. Sci.*, 2007, **96**, 705–728.
4 S. R. Byrn, R. R. Pfeiffer and J. G. Stowell, *Solid State Chemistry of Drugs*, SSCI, Inc., West Lafayette, IN, 2nd edn, 1999.
5 R. Hilfiker, *Polymorphism: in the Pharmaceutical Industry*, Wiley-VCH, Weinheim, 2006.
6 W. C. McCrone, in *Physics and Chemistry of the Organic Solid State*, ed. D. L. Fox, M. M. Labes and A. Weissberger, Wiley-VCH, New York, 1965, vol. 2, pp. 725–767.
7 G. T. Beckham, B. Peters and B. L. Trout, *J. Phys. Chem. B*, 2008, **112**, 7460–7466.
8 P. Ectors, P. Duchstein and D. Zahn, *Cryst. Growth Des.*, 2014, **14**, 2972–2976.
9 M. I. Tamboli, S. Krishnaswamy, R. G. Gonnade and M. S. Shashidhar, *Cryst. Growth Des.*, 2014, **14**, 4985–4996.
10 S. Wishkerman and J. Bernstein, *Chem. – Eur. J.*, 2008, **14**, 197–203.
11 J. Zhang, Y. Wu, A. Liu, W. Li and Y. Han, *RSC Adv.*, 2014, **4**, 21599–21607.
12 A. Llinas and J. M. Goodman, *Drug Discovery Today*, 2008, **13**, 198–210.
13 Y. Mo, L. Dang and H. Wei, *Ind. Eng. Chem. Res.*, 2011, **50**, 10385–10392.
14 V. Lopez-Mejias, J. W. Kampf and A. J. Matzger, *J. Am. Chem. Soc.*, 2012, **134**, 9872–9875.
15 R. Hiremath, J. A. Basile, S. W. Varney and J. A. Swift, *J. Am. Chem. Soc.*, 2005, **127**, 18321–18327.
16 X. Yang, B. Sarma and A. S. Myerson, *Cryst. Growth Des.*, 2012, **12**, 5521–5528.
17 X. Sun, B. A. Garetz and A. S. Myerson, *Cryst. Growth Des.*, 2006, **6**, 684–689.
18 R. G. Della Valle, E. Venuti, A. Brillante and A. Girlando, *J. Phys. Chem. A*, 2008, **112**, 1085–1089.
19 A. J. Misquitta, G. W. A. Welch, A. J. Stone and S. L. Price, *Chem. Phys. Lett.*, 2008, **456**, 105–109.
20 M. A. Neumann, *J. Phys. Chem. B*, 2008, **112**, 9810–9829.
21 M. A. Neumann, F. J. J. Leusen and J. Kendrick, *Angew. Chem., Int. Ed.*, 2008, **47**, 2427–2430.
22 S. L. Price, *Phys. Chem. Chem. Phys.*, 2008, **10**, 1996–2009.
23 S. L. Price, *Chem. Soc. Rev.*, 2014, **43**, 2098–2111.
24 M. Vasileiadis, C. Pantelides and C. S. Adjiman, *Chem. Eng. Sci.*, 2015, **121**, 60–76.
25 J. Bernstein, in *Organic Solid State Chemistry*, ed. G. R. Desiraju, Elsevier, Amsterdam, 1987, vol. 32, pp. 471–518.
26 A. Nangia, *Acc. Chem. Res.*, 2008, **41**, 595–604.
27 A. J. Cruz-Cabeza and J. Bernstein, *Chem. Rev.*, 2014, **114**, 2170–2191.
28 S. Long, S. Parkin, M. Siegler, C. P. Brock, A. Cammers and T. Li, *Cryst. Growth Des.*, 2008, **8**, 3137–3140.
29 S. Long, S. Parkin, M. Siegler, A. Cammers and T. Li, *Cryst. Growth Des.*, 2008, **8**, 4006–4013.
30 S. Long, M. Siegler and T. Li, *Acta Crystallogr., Sect. E: Struct. Rep. Online*, 2007, **63**, o279–o281.

31 S. Long and T. Li, *Cryst. Growth Des.*, 2009, **9**, 4993–4997.
32 S. Long and T. Li, *Cryst. Growth Des.*, 2010, **10**, 2465–2469.
33 S. Long, P. Zhou, S. Parkin and T. Li, *Cryst. Growth Des.*, 2014, **14**, 27–31.
34 C. Hoarau, A. Couture, H. Cornet, E. Deniau and P. Grandclaudon, *J. Org. Chem.*, 2001, **66**, 8064–8069.
35 *Nonius, COLLECT and EVAL*, Nonius BV, Delft, the Netherlands, 2002.
36 Z. Otwinowski and W. Minor, in *Methods in Enzymology: Macromolecular Crystallography, Part A*, ed. C. W. Carter Jr. and R. M. Sweet, Academic Press, New York, 1997, vol. 276, pp. 307–326.
37 G. M. Sheldrick, *Acta Crystallogr., Sect. A: Found. Crystallogr.*, 2008, **64**, 112–122.
38 M. J. Frisch, G. W. Trucks, H. B. Schlegel, G. E. Scuseria, M. A. Robb, J. R. Cheeseman, G. Scalmani, V. Barone, B. Mennucci, G. A. Petersson, H. Nakatsuji, M. Caricato, X. Li, H. P. Hratchian, A. F. Izmaylov, J. Bloino, G. Zheng, J. L. Sonnenberg, M. Hada, M. Ehara, K. Toyota, R. Fukuda, J. Hasegawa, M. Ishida, T. Nakajima, Y. Honda, O. Kitao, H. Nakai, T. Vreven, J. A. Montgomery, Jr., J. E. Peralta, F. Ogliaro, M. Bearpark, J. J. Heyd, E. Brothers, K. N. Kudin, V. N. Staroverov, R. Kobayashi, J. Normand, K. Raghavachari, A. Rendell, J. C. Burant, S. S. Iyengar, J. Tomasi, M. Cossi, N. Rega, N. J. Millam, M. Klene, J. E. Knox, J. B. Cross, V. Bakken, C. Adamo, J. Jaramillo, R. Gomperts, R. E. Stratmann, O. Yazyev, A. J. Austin, R. Cammi, C. Pomelli, J. W. Ochterski, R. L. Martin, K. Morokuma, V. G. Zakrzewski, G. A. Voth, P. Salvador, J. J. Dannenberg, S. Dapprich, A. D. Daniels, O. Farkas, J. B. Foresman, J. V. Ortiz, J. Cioslowski and D. J. Fox, *Gaussian 09, Revision, A. 02*, Gaussian, Inc., Wallingford CT, 2009.
39 Y. Zhao and D. G. Truhlar, *J. Chem. Phys.*, 2006, **125**, 194101.
40 Y. Zhao and D. G. Truhlar, *Acc. Chem. Res.*, 2008, **41**, 157–167.
41 Y. Zhao and D. G. Truhlar, *Theor. Chem. Acc.*, 2008, **120**, 215–241.
42 S. Feng and T. Li, *J. Chem. Theory Comput.*, 2006, **2**, 149–156.
43 T. Li and S. Feng, *Pharm. Res.*, 2006, **23**, 2326–2332.
44 R. Dovesi, R. Orlando, B. Civalleri, C. Roetti, V. R. Saunders and C. M. Zicovich-Wilson, *Z. Kristallogr.*, 2005, **220**, 571–573.
45 S. F. Boys and F. Bernardi, *Mol. Phys.*, 1970, **19**, 553–566.
46 Z. Berkovitchyellin and L. Leiserowitz, *J. Am. Chem. Soc.*, 1982, **104**, 4052–4064.
47 M. Fujinaga and M. N. G. James, *Acta Crystallogr., Sect. B: Struct. Crystallogr. Cryst. Chem.*, 1980, **36**, 3196–3199.
48 S. Long, M. Siegler and T. Li, *Acta Crystallogr., Sect. E: Struct. Rep. Online*, 2006, **62**, O5664–O5665.
49 J. Bernstein, R. E. Davis, L. Shimoni and N.-L. Chang, *Angew. Chem., Int. Ed. Engl.*, 1995, **34**, 1555–1573.
50 F. Takusagawa and A. Shimada, *Acta Crystallogr., Sect. B: Struct. Crystallogr. Cryst. Chem.*, 1976, **32**, 1925–1927.